Seasonality of Global and Arctic Black Carbon Processes in the AMAP Models

Rashed Mahmood[1,2], Knut von Salzen[1,3,*], Mark Flanner[4], Maria Sand[5], Joakim Langner[6], Hailong Wang[7], and Lin Huang[8]

[1]School of Earth and Ocean Sciences, University of Victoria, Victoria, British Columbia, Canada

[2]Department of Meteorology, COMSATS Institute of Information Technology, Islamabad, Pakistan

[3]Canadian Center for Climate Modelling and Analysis, Environment and Climate Change Canada, University of Victoria, Victoria, British Columbia, Canada

[4] Department of Atmospheric, Oceanic and Space Sciences, University of Michigan, Michigan, USA

[5]Center for International Climate and Environmental Research -Oslo (CICERO), Oslo, Norway

[6]Swedish Meteorological and Hydrological Institute, Norrköping, Sweden

[7]Atmospheric Sciences and Global Change Division, Pacific Northwest National Laboratory, Richland, Washington, USA

[8]Climate Chemistry Measurements and Research, Environment and Climate Change Canada, Toronto, Ontario, Canada

[*]Corresponding author:

Knut von Salzen,

This is the author manuscript accepted for publication and has undergone full peer review but has not been through the copyediting, typesetting, pagination and proofreading process, which may lead to differences between this version and the Version of Record. Please cite this article as doi: 10.1002/2016JD024849

Canadian Centre for Climate Modelling and Analysis (CCCma), Environment and Climate Change Canada

University of Victoria, PO Box 1700, STN CSC, Victoria, BC V8W 2Y2

Phone: 250 363-8237

Email: knut.vonsalzen@canada.ca

Key Points:

Seasonal variations of black carbon (BC) mass budgets in the Arctic are simulated

Good agreement in simulated annual mean transport of BC to the Arctic in models

Convective wet removal is important for differences in modeled BC concentration

Abstract

This study quantifies black carbon (BC) processes in three global climate models and one chemistry transport model, with focus on the seasonality of BC transport, emissions, wet and dry deposition in the Arctic. In the models, transport of BC to the Arctic from lower latitudes is the major BC source for this region. Arctic emissions are very small. All models simulated a similar annual cycle of BC transport from lower latitudes to the

Arctic, with maximum transport occurring in July. Substantial differences were found in simulated BC burdens and vertical distributions, with CanAM (NorESM) producing the strongest (weakest) seasonal cycle. CanAM also has the shortest annual mean residence time for BC in the Arctic followed by SMHI-MATCH, CESM and NorESM. Overall, considerable differences in wet deposition efficiencies in the models exist and are a leading cause of differences in simulated BC burdens. Results from model sensitivity experiments indicate that convective scavenging outside the Arctic reduces the mean altitude of BC residing in the Arctic, making it more susceptible to scavenging by stratiform (layer) clouds in the Arctic. Consequently, scavenging of BC in convective clouds outside the Arctic acts to substantially increase the overall efficiency of BC wet deposition in the Arctic, which leads to low BC burdens and a more pronounced seasonal cycle compared to simulations without convective BC scavenging. In contrast, the simulated seasonality of BC concentrations in the upper troposphere is only weakly influenced by wet deposition in stratiform clouds whereas lower tropospheric concentrations are highly sensitive.

Keywords: black carbon budgets, transport, wet scavenging, aerosols, Arctic pollution

1 Introduction

The light absorbing component of carbonaceous aerosols known as black carbon (BC) is emitted into the atmosphere by incomplete combustion processes and open biomass/biofuel burning [*Bond et al*., 2004]. BC affects the climate through broad mechanisms referred to as direct, semi-direct and indirect effects [*Jacobson*, 2001; *Bond et al*., 2013; *Boucher et al*., 2013]. The direct radiative effect is related to the scattering and absorption of solar radiations by BC. Absorption of radiation by BC within clouds and surrounding clear air can modify the distribution of clouds, a phenomenon known as the semi-direct effect [*Hansen et al*., 1997]. Indirect effects are associated with modifications of cloud properties [e.g. *Koch et al.*, 2011]. BC can also increase the melt rate of snow by enhanced absorption of solar radiation by BC in snow [*Hansen and Nazarenko*, 2004]. A recent study by *Bond et al*. [2013] has estimated a total BC climate forcing for the industrial era (including all processes) of +1.1 W/m^2 (+0.17 to +2.1 W/m^2), implying that BC may be the second largest global warming agent after carbon dioxide. The total forcing, however, could be much smaller when co-emitted aerosol species are considered [*Bond et al*., 2013].

The strong heating potential and short atmospheric residence time of BC (about one week) offers rapid global warming mitigation opportunities. However, the large uncertainty range associated with the estimated BC forcing leads to substantial challenges in effective decision making. Moreover, the radiative effects of BC vary with location on Earth, with considerable impacts expected near the source regions and the Arctic [e.g., *Sand et al*., 2013]. Part of the uncertainty in climate forcing on global as well as regional

scales is associated with simulations of the horizontal and vertical distribution of BC in models [e.g. *Allen and Landuyt*, 2014; *Samset et al*., 2014; *Hodnebrog et al*., 2014; *Kipling et al*., 2015]. For the Arctic region, the observed seasonal cycle of BC surface concentrations has peak values in winter and spring seasons [*Sharma et al*., 2006; *Garrett et al*., 2010, 2011]. Lower concentrations during summer are partly caused by the northerly location of the 'Arctic front', which is a transport barrier that isolates the Arctic lower troposphere from lower latitudes [*Barrie*, 1986; *Stohl*, 2006]. Pollution emitted south of the Arctic front can reach the Arctic by advection following sloping surfaces of constant potential temperature. This is the main transport mechanism by which emissions from eastern North America and southeastern Asia can reach the Arctic [*Stohl*, 2006]. However, *Garrett et al*. [2010, 2011] concluded that low concentrations in summer are mainly caused by efficient wet scavenging of BC during transport from low latitudes to the Arctic. While many models qualitatively reproduce the seasonal cycle of BC in the Arctic, the amplitudes of the simulated seasonal cycle remain inconsistent with observations [e.g., *Shindell et al*., 2008; *Eckhardt et al*., 2015]. This may be related to the representation of different aerosol processes, such as the relative contribution of wet and dry deposition [e.g., *Vignati et al*., 2010], aging [e.g., *Liu et al*., 2011, 2016], different scavenging efficiencies by different types of clouds [e.g., *Browse et al*., 2012; *Wang et al*., 2013] and model resolution [e.g. *Ma et al*., 2014]. On the other hand, *Ma et al*. [2013] found that simulated circulation features regulating BC transport are unlikely to affect

surface concentrations of BC in the Arctic in the Community Atmosphere Model version 5 (CAM5).

The purpose of this study is to quantify BC budgets in the Arctic region in models that were used for a recent assessment of Arctic aerosols and climate by the Arctic Monitoring and Assessment Programme [*AMAP*, 2015; *Sand et al.*, 2015], which addressed impacts of emissions of BC and other short-lived climate forcers from different regions and economic sectors on Arctic temperatures. Key results of the assessment were based on an analysis of results from simulations with models that were developed by modelling groups in different Arctic nations. As an extension to AMAP assessment activities, the study here focuses on seasonal cycles of BC processes and concentrations in the Arctic. Specifically, contributions of transport, wet and dry removal processes to simulated Arctic BC burdens in AMAP models are analyzed. The relative importance of wet and dry removal processes and the vertical distribution of BC are also explored. The current study focuses on atmospheric BC burdens in the Arctic, which are arguably more relevant to radiative effects of BC on climate than surface concentrations, frequently considered in the literature. As will be demonstrated in the following, differences in simulated BC burdens in models are caused by relatively small differences in mass budgets which cannot be fully understood without a comprehensive assessment of all sources and sinks of BC in the models, including the influence of transport on BC burdens.

2 Methods

This study uses data sets from three different global climate models and one chemistry transport model (see Table 1). Simulations conducted with the Community Earth System Model (CESM) utilize the Community Atmosphere Model version 5.2 (CAM 5.2) atmospheric component with modal aerosol module (MAM) treatment [*Liu et al.*, 2012], including important modifications to the aerosol wet scavenging processes that result in substantially more aerosol transport to the Arctic [*Wang et al*., 2013]. Here, we use the 7 mode version of MAM that simulates BC in two modes, a feature that leads to slower removal of BC [e.g., *Liu et al.*, 2012]. BC is initially emitted to the primary carbon mode and subsequently enters to the accumulation mode due to the condensation and coagulation of other aerosol species and aerosol precursors. Wet deposition of cloud-borne and interstitial aerosols is based on modified versions of wet removal routines from previous work [*Rasch et al.*, 2000; *Barth et al*., 2000]. In-cloud scavenging depends on the aerosol hygroscopicity, cloud condensate mixing ratio and cloud fraction, and cloud-borne aerosols are then removed proportionately with conversion of cloud condensate to precipitation [e.g., *Neale et al.*, 2012]. Below-cloud removal of interstitial aerosols depends on the precipitation rate and size- and species-specific aerosol scavenging efficiencies that implicitly account for impaction and Brownian motion. Improvements by *Wang et al*. [2013] include self-consistent treatment of vertical transport and aerosol wet removal in convective updrafts, secondary activation of laterally entrained aerosols

above convective cloud base, more physically-based treatment of liquid cloud fraction in mixed-phase clouds, and in-cloud scavenging efficiency.

The Norwegian Earth System Model [NorESM, *Berntsen et al*., 2013] is primarily based on the National Center for Atmospheric Research (NCAR) Community Climate System Model version 4 (CCSM4) which includes a modified version of CAM4 as an atmospheric model (CAM4-Oslo). The aerosol module in CAM4-Oslo separately represents aerosols, aerosol-cloud interactions and aerosol radiative effects [*Kirkevåg et al*., 2013]. The aerosol mass concentrations are calculated using a simple aerosol life cycle scheme [*Iversen and Seland*, 2002, 2003; *Seland et al*., 2008]. The mass concentrations are tagged based on production mechanisms for each of the four (i.e. nucleation, aitken, accumulation and coarse) size modes. BC is emitted as primary particle in two modes and also as internally mixed with organic matter in one mode. Details of dry and wet removal processes and the removal coefficients for the aerosols in different modes have been summarized in *Seland et al*. [2008, Table 2 and section 2.4].

The Swedish Meteorological and Hydrological Institute Multi-scale Atmospheric and Chemistry Transport model (SMHI-MATCH) [*Robertson et al*., 1999] is an offline 3D chemistry transport model. SMHI-MATCH can be run on both global and regional domains but for this study model runs were performed for the ~20°N-90°N region. SMHI-MATCH with gas-phase chemistry and bulk aerosols considering 63 species using 130 chemical reactions was used [*Andersson et al.*, 2007]. The aerosol scheme was

extended with BC and OC simulated as two fractions: fresh, hydrophobic and aged, hydrophilic. 80% of anthropogenic emissions from all sectors were emitted into the hydrophobic and 20% into the hydrophilic fraction except for fire/biomass combustion where 100% was emitted into the hydrophilic component following *Genberg et al.* [2013]. Scavenging and ageing was parameterized following *Liu et al.* [2011], i.e. ageing is proportional to OH and scavenging in mixed-phase clouds is reduced. The hydrophobic fraction is assumed to be 5% activated in the scavenging scheme, while the hydrophilic fraction is 100% activated. If the clouds are mixed phase the scavenging efficiency is scaled by the ratio of cloud ice water content to total cloud water content assuming zero scavenging for 100% ice clouds. We used ERA-Interim re-analysis data from ECMWF to drive SMHI-MATCH for the years 2006-2010. Six-hourly data (3 hourly for precipitation) were extracted from the ECMWF archives on a 0.75° × 0.75° rotated latitude–longitude grid. The original data had 60 levels, but the 35 lowest levels reaching about 16 km in the Arctic were used in the model.

Version 4.2 of the Canadian Atmospheric Global Climate Model (CanAM) is used, with calculations of aerosol microphysical processes based on the Piecewise Lognormal Approximation [PLA, *von Salzen*, 2006]. Compared to version 4 of CanAM [*von Salzen et al*., 2013], a higher vertical resolution and improved parameterizations are employed for aerosol processes, clear-sky radiative transfer, DMS emissions, land surface and snow processes. Similar to version 4, aerosol processes in convective and layer clouds are represented using separate parameterizations in the model. Deep and

shallow convective clouds are represented using mass-flux schemes with interactive calculations of convective transport processes (updrafts, downdrafts, entrainment, and detrainment) and in-cloud scavenging of aerosols by conversion of cloud liquid water to rain [*von Salzen et al*., 2000]. In-cloud convective wet removal efficiency (solubility) factors of 0.9 and 0 are used for hydrophilic and hydrophobic BC, respectively. Aerosol processes in layer clouds include in- and below-cloud scavenging, in-cloud oxidation, and rain evaporation. Calculations of in-cloud and clear-sky production of sulphate aerosol are based on specified monthly mean oxidation concentrations. BC is predominantly emitted as an externally mixed and hydrophobic aerosol species which subsequently ages to internally mixed hydrophilic BC in the atmosphere, with a daylight-dependent aerosol lifetime.

All models use anthropogenic emissions for BC, organic carbon and sulphur for year 2010 from the ECLIPSE inventory, version 4a [*Stohl et al.*, 2015; *AMAP*, 2015] and monthly varying emissions for forest and grass fires from GFED, version 3.1 [*van der Werf*, 2010], which were converted to the model grid by each modelling group. The models were integrated for 2006-2010, with specified sea surface temperatures, sea ice concentrations, GHG concentrations, and volcanic forcings during this time period. Results are presented as monthly and seasonal means for the last four years of the model simulations (i.e. 2007-2010) leaving 2006 for model spin-up. In addition, high-frequency model data for vertical BC distributions for years 2008 and 2009 were available for selected locations. For consistency, the model outputs from different models were

remapped to a uniform 1°×1° grid using first order conservative interpolation (Ramshaw, 1985). Similarly, for vertical profiles, the model outputs were vertically interpolated for a set of uniform pressure levels. We chose the Arctic region as the area north of the Arctic Circle (67°N-90°N). Results for lower latitudes are also considered in the following for a more comprehensive assessment of the models. In the following, mass budgets of BC in the Arctic will be determined based on monthly mean output from the models, ,

$$\frac{db}{dt} = E + T + (D + W_L + W_C)\,, \qquad (1)$$

where *b* denotes the burden of BC , *E* the emission flux, *T* transport (advection and horizontal diffusion), *D* dry deposition plus gravitation settling, and W_L /W_C wet deposition in layer/convective clouds, respectively. The known terms in Eq. (1) are the net BC surface fluxes (*E*, *D*, W_L, W_C) and storage of BC mass ($\frac{db}{dt}$). The latter is obtained from the differences in burdens between month boundaries (i.e. beginning of first day of a month). The horizontal BC transport (*T*) is diagnosed as a residual term in the BC mass budget equation. Hence, an advantage of this approach is that it relies on data that are readily available from models. In addition, time scales of BC processes were calculated as the ratio of mean BC burden over mean, vertically integrated BC fluxes and are expressed in units of time.

3 Results and Discussion

3.1 Simulation of BC in the Arctic in AMAP models

Fig. 1 shows simulated seasonal mean BC burdens in the Arctic region (67°N-90°N). CESM and SMHI-MATCH produce maxima in winter while CanAM and NorESM produce maxima in spring. All models, except NorESM, simulate markedly lower burdens in summer and fall. Overall, the decrease in BC burden from spring to fall is more pronounced in CanAM and SMHI-MATCH than in CESM and NorESM. The seasonality in BC burden in NorESM is particularly weak, with very high BC burdens in summer and fall seasons compared to other models.

Simulated BC direct radiative forcings, and ultimately Arctic climate impacts (*AMAP*, 2015), are strongly related to BC burdens and optical properties between spring and fall equinoxes. For instance, Arctic direct radiative forcing and BC burden are higher for NorESM (Table 2) than for any other AMAP model. However, SMHI-MATCH produces slightly larger BC burden than CanAM and relatively weak radiative forcing. The reason for this is not known but it seems plausible that these differences are either associated with differences in simulated aerosol optical properties and/or the differences in the distribution of aerosols relative to clouds in the models.

Simulated BC concentrations from AMAP and other models were recently compared to observations by *Eckhardt et al*. [2015] and *AMAP* [2015] based on comprehensive data sets from surface sites and aircraft campaigns. Identical AMAP model configurations and emission data sets were used by *Eckhardt et al*. and for the current study so that findings by *Eckhardt et al*. are directly relevant to discussions here. In summary, Eckhardt et al.

show that observed BC near-surface concentrations have a distinct seasonal cycle with high values in winter/spring and low values in summer at various Arctic sites. All AMAP models broadly reproduce the observed seasonality of BC near-surface concentrations. However, the models tend to underestimate the magnitude of BC near-surface concentrations, especially during the most highly polluted months of the year. This bias appears to be more significant in NorESM and CESM while CanAM produces particularly reasonable agreement with the observations, especially during the spring season. Comparisons of model results with aircraft measurements do not provide any evidence for large systematic overestimates of simulated BC concentrations in the upper troposphere in the Arctic in the AMAP models, which is different from conclusions in several previous studies [e.g. *Koch et al.*, 2009; *Kipling et al.*, 2013; *Wang et al.*, 2013; *Allen and Landuyt*, 2014; *Samset et al.*, 2014]. Furthermore, *Eckhardt et al.* [2015] concluded that substantial variability in aircraft measurements and model results arises from the fact that some campaigns targeted biomass burning plumes while others avoided such plumes, which affects the robustness of climatologically meaningful comparisons with models. Generally, comparisons of vertical profiles are currently limited by a lack of horizontal, vertical, and long-term coverage of aircraft campaigns, which is problematic given the substantial variability in Arctic BC concentrations. Consequently, additional comparisons are needed for further validation of simulations of BC and climate which are well beyond the scope of this study. However, comparisons between models and observations can be expected to benefit from consideration of particularly uncertain

aerosol and atmospheric processes which cause the largest differences in simulated BC concentrations and associated climate effects in models. As a step towards this objective, a systematic analysis of Arctic BC processes and their differences in AMAP models will be presented in the following.

3.2 BC Budgets in Models

BC burdens are influenced by a range of different processes. Fig. 2 shows simulated BC burdens and mass budgets for 5 different latitude bands (i.e., 67N-90°N, 20°N-67°N, 20°S-20°N, 67°S-20°S, 90°S-67°S) and global values for each model and month, averaged over all years of the simulation (i.e. 2007-2010). In Fig. 2, the net BC surface source (net total BC flux from emissions and deposition in a region) is compared to the net transport.

As shown in Fig. 2, simulated BC budgets and burdens over BC source regions at low and mid latitudes are similar in all models, especially in the tropics (20°S-20°N). However, significant differences, especially in BC burdens, occur at high latitudes in both hemispheres. In the Arctic, peak BC burdens occur in April, January, and July in CanAM, CESM/SMHI-MATCH and NorESM respectively, with the overall strongest seasonal cycle simulated by CanAM and weakest by NorESM.

The main source of BC in the Arctic is long-range transport from regions at lower latitudes. In winter, BC is transported efficiently from the main source region (20°N-

67°N) to regions at higher and lower latitudes in all models (Fig. 2). In the spring, especially March and April, transport out of this source region is relatively inefficient (Fig. S1 in supplementary document), which can likely be explained by weak meridional winds over continental source regions during these months. However, net transport to the Arctic region (67°N-90°N) from lower latitudes is still positive (Fig. 2). In late summer, transport out of the main source region (20°N-67°N) becomes stronger again, with decreasing time scale (increasing efficiency) of transport towards the tropics as the summer progresses (Fig. S1). In the fall, a strong net export of BC from the source regions in the northern hemisphere to the southern hemisphere is established (Fig. 2), as can be seen in peak values of transport in the southern hemisphere (67°S-20°S) during the fall. The reason for the increase in transport of BC from the northern to the southern hemisphere is not clear. Efficient transport of carbon monoxide, carbon dioxide, and ozone from the northern to the southern hemisphere has been attributed to seasonal variations in circulation and transient wave propagation in the upper troposphere [*Staudt et al*., 2001; *Sudo and Akimoto*, 2007; *Sawa et al*., 2012]. Cross-hemisphere transport of biomass pollutants also has been reported previously [e.g. *Real et al*., 2010]. It seems plausible that transport of BC between both hemispheres occurs through similar transport pathways. Using an explicit BC source tagging technique, *Wang et al.* (2014) showed that a significant portion (over 20%) of annual mean BC burden in the southern hemisphere originates from sources in the northern hemisphere.

All seasons experience net transport of BC from lower latitudes to the Arctic region. The annual mean transport is very similar in all models, with lowest values in CESM (0.133 kilotonnes per day [kt/day]) and highest in CanAM (0.155 kt/day, Table S1 in supplementary document). The transport to the Arctic region is strongest in July, which is locally caused by large vegetation fire emissions near ~60° N (Fig. S2). A secondary peak in transport occurs during winter and is associated with efficient transport of polluted air masses from industrialized regions, which are often located within the polar circulation system during winter [*Stohl*, 2006] and decreased scavenging efficiency due to a predominance of mixed and ice-phase clouds [*Liu et al*., 2011; *Browse et al*., 2012]. All models produce minima in transport to the Arctic during late spring and early fall, which are particularly pronounced in CanAM and SMHI-MATCH. In general, minima in transport are associated with minima in BC burdens in the models. The main exception is CanAM, which produces a springtime maximum in BC burdens, partly owing to a short time scale of transport of BC to the Arctic during previous months (Fig. S1).

In the annual mean, transport and emission sources of BC in the Arctic are well balanced by dry and wet deposition of BC (Table S1). Similar to transport, there is good agreement in simulated dry and wet deposition fluxes among the models, with wet deposition rates contributing 62%, 67.6%, 68.1%, and 86.6% to total deposition in CanAM, CESM, NorESM and SMHI-MATCH respectively (Fig. S3). No obvious correlation with simulated burdens is found. These results indicate that the substantial differences in simulated annual mean Arctic BC burdens might be a consequence of

rather subtle differences in deposition processes and likely cannot be explained by annual mean BC mass budgets, including differences in net BC transport to the Arctic.

3.3 Efficiencies of Arctic BC Processes

BC burdens in the Arctic in the models are clearly related to aerosol microphysical process time scales in the Arctic, with particularly short and long time scales of wet deposition in CanAM and in NorESM, respectively (Fig. S1 and Table S2). The annual mean residence time of BC for the Arctic region, i.e. the ratio of BC burden over burden change due to total (dry and wet) deposition, is about a factor of two higher in NorESM than in CanAM. In order to quantify these differences in more detail, the following analysis will focus on seasonal variations in BC deposition rates and time scales.

There are substantial seasonal variations in simulated dry and wet deposition rates as shown in Fig. 3. During winter, precipitation is low (Fig. S4) and dry deposition is more efficient in removing BC from the Arctic atmosphere than during any other season, as simulated by all models. Dry deposition is more important than wet deposition in CanAM during winter. In contrast, dry and wet deposition rates are of comparable magnitude in CESM and NorESM. SMHI-MATCH produces the largest wintertime wet deposition flux of all models (Fig. 3). Less than half of the BC that reaches the Arctic by transport is removed by wet deposition in CanAM, which is much less than in the other models in winter (Fig. 3). Although CanAM produces a relatively large dry deposition flux compared to the other models in winter, this does not compensate for the weak wet

deposition flux so that the net source of BC in the Arctic is strongly positive in CanAM. For SMHI-MATCH, a small dry deposition flux compared to other models contributes to a net positive source of BC, mainly in early winter (Fig. 2).

During spring, wet deposition becomes more important in all models and accounts for 52.9%, 70.5%, 64.7%, and 88% of total deposition in CanAM, CESM, NorESM, and SMHI-MATCH, respectively. The relatively large wet deposition fluxes in CESM and SMHI-MATCH and weaker transport (Fig. S3) lead to a decline in BC burdens in these models. However, wet deposition is less important and burdens are nearly steady in CanAM and NorESM.

During summer and fall, precipitation rates for lower tropospheric clouds are higher than during other seasons (Fig. S4), leading to high wet deposition fluxes in all models (Fig 3), which agrees with conclusions by *Garrett et al.* [2010, 2011] about the strong impact of wet deposition on seasonal variations of Arctic BC burdens. The particularly high efficiency of wet deposition is also evident from the particularly short simulated time scales of wet deposition during summer and fall (Fig. S1). This causes BC burdens to decline over the summer in all models, especially in CanAM, which produces a particularly large reduction in the time scale of wet deposition from spring. During the transition from late summer/fall to winter, wet deposition becomes weaker and less efficient in all models and BC burdens start to increase in CanAM, CESM, and SMHI-MATCH but still remain nearly steady in NorESM (Fig. 2).

Overall, seasonal variations in the magnitudes and time scales of sources and sinks of BC are weaker in NorESM than in the other models (Fig. S1), especially compared to CanAM (if periods with impacts of forest fires at high latitudes are disregarded). This is consistent with seasonal variations in BC burdens (cf. Fig. 1 and Fig. 3), which are also relatively weak in NorESM compared to other models and especially CanAM. A key difference between NorESM and CanAM/SMHI-MATCH appears to be the particularly long time scale of wet deposition during summer in NorESM (Fig. S1). This may at least partly explain the high BC burdens in NorESM during this time of the year (Fig. 1) and in the annual mean (Table S1). In contrast, CanAM and SMHI-MATCH produce much higher wet deposition efficiencies during summer.

Differences in wet deposition efficiencies do not seem to be related to precipitation rates (Fig. S4). In particular, precipitation in CanAM in summer is generally lower than in NorESM, which does not appear to be consistent with a relatively short time scale of wet deposition in CanAM from in- and below-cloud scavenging processes.

It is interesting to note that global BC burdens and total deposition rates are relatively similar in all models (Table S1). However, differences in individual contributions of wet and dry deposition rates are more pronounced. For instance, the contributions of wet to total deposition rates are 83.3%, 74.4%, and 68.1% in CanAM, CESM, and NorESM, respectively, which provides further evidence for globally more efficient wet deposition in CanAM than in CESM and NorESM.

There are also some systematic differences in budgets among the models for the Antarctic region (defined here as 67°S to 90°S, Fig. 2). Similar to the Arctic, NorESM produces much higher burdens than CanAM. This seems to be partly caused by relatively long time scale of wet deposition in NorESM in this region (Table S2 and Fig. S1). This is consistent with Arctic and global results. In addition, Fig. 2 shows that NorESM also has by far the strongest transport to this region, followed by CESM and CanAM, which presumably is a consequence of inefficient wet deposition of BC at lower latitudes.

In order to further characterize how seasonal variations in Arctic BC burdens are related to individual processes it is useful to relate changes in BC burdens to time scales of wet and dry deposition. The following expression can be directly derived from Eq. (1):

$$\frac{db}{dt} = E + T - b\left(\frac{1}{\tau_d} + \frac{1}{\tau_w}\right), \qquad (2)$$

where τ_d and τ_w are time scales of dry and wet deposition, respectively. Eq. (2) provides a framework for a simple conceptual model of BC burdens in the Arctic atmosphere which can be exploited to interpret temporal changes in BC burdens in AMAP models. In particular, the conceptual model can be used to investigate the sensitivity of BC burden changes to emissions, transport, and deposition. In the following this model is used to interpret and characterize the role of processes in AMAP models. Multi-year mean results during the time period from April 1 to September 30 will be considered because this time period is characteristic of the marked transition from high burdens to low burdens in fall

in most of the model. In addition, simulated rates of reduction in the models differ over this time period but initial BC burdens are similar on April 1 so that a comparison is meaningful with regard to characterization of model differences.

Mean simulated sources and sinks of BC during the time period April 1 to September 30 in the AMAP models are provided in Table 3. These were used to determine τ_d and τ_w in Table 3 based on an analytical solution of Eq. (2). The results agree well with time scales that were determined based on monthly results from the models during this time period (Fig. S1).

Removal of Arctic emissions and transport terms from the conceptual model yields decreases in BC burdens that are more rapid than in the full models, especially for removal of transport. This indicates that these sources of BC in the Arctic act to weaken the seasonal decline in BC burdens, as can be expected from the BC mass budget (Table 4). The impact on the seasonal decline is particularly large for NorESM, which points at a relatively large sensitivity of simulated BC burden changes to emissions and transport in NorESM. In contrast, BC burden changes are much less sensitive to these processes for CanAM.

The omission of wet deposition in the models leads to rapid increases in BC burdens for all models, especially for NorESM (Table 4). BC burden changes are much more sensitive to the removal of wet deposition from the calculations than to the removal of Arctic emissions, transport, or dry deposition in the conceptual model, independent of the

choice of model. Therefore, differences in wet deposition time scales appear to be particularly important with regard to overall differences in simulated seasonal changes in BC burdens. Clearly, changes associated with removal of dry deposition are much weaker than changes associated with the removal of wet deposition for all models.

It is also useful to consider the multi-model range of processes from the models and determine BC burdens changes in the conceptual model that correspond to simulated minimum and maximum values of sources and sinks given in Table 3. For each model the minimum or maximum values of a specific source or sink can be combined with other source and sink terms to calculate change in burden in that model. For instance, transport of BC to the Arctic is particularly weak (i.e. minimum) in SMHI-MATCH and particularly strong (i.e. maximum) in NorESM (Table 3). It is useful to determine the response of the BC burden change for NorESM if sources and sinks terms of NorESM are combined with weak transport from SMHI-MATCH. Interestingly, the substitution of the transport source in NorESM still produces a relatively weak seasonal decrease in simulated BC burden for NorESM compared to other models and the multi-model mean, despite much weaker transport in SMHI-MATCH (Table 4). Hence, differences in transport in models only partly account for differences in BC burden changes between NorESM and other models. However, differences in wet deposition time scales appear to explain most of the differences in simulated BC burden changes among AMAP models (Table 4). All models produce similar ranges in simulated BC burden changes for given minimum and maximum wet deposition time scales, despite considerable differences in

simulated Arctic emissions, transport, and dry deposition in individual models. This indicates that the models could potentially produce similar seasonal changes in BC burdens if similar removal efficiencies of BC by wet deposition are simulated in the AMAP models.

In summary, calculations with a simple conceptual model that are constrained by sources and sinks of BC in the Arctic from simulations with AMAP models indicate that differences in simulated seasonal cycles of BC in the Arctic are mainly caused by differences in the efficiency of wet deposition in the models. The role of wet deposition and other processes for the simulated seasonality of BC vertical profiles will be analyzed in more detail in the following.

3.4 Sensitivity of BC Vertical Concentration Profiles to Aerosol Processes

Differences in time scales of wet deposition in the Arctic in models may be caused by differences in parameterizations of BC scavenging in Arctic clouds or spatio-temporal correlations of precipitating clouds and BC concentrations. Large differences in wet deposition efficiencies during summer and fall point at a potential role of local cloud processes in the Arctic for model differences because precipitation rates are particularly high relative to other seasons and BC residence times are short.

To further illustrate the differences in model results for the Arctic, annual mean vertical distributions of BC at Alert, Canada are shown in Fig. 4a. Results for other sites

in the Arctic are similar and are not shown here. CanAM produces a BC concentration maximum in the lower troposphere while all the other models produce maxima somewhere between the middle and upper troposphere. Further, Figs. 4b and 4c provide monthly varying vertically integrated BC concentrations for the troposphere (1000-250 hPa) and upper troposphere/stratosphere (250-10 hPa) respectively. BC concentrations in the troposphere (Fig. 4b) are highest during spring compared to other seasons in CanAM, CESM and NorESM while SHMI-MATCH simulates a wintertime maximum. During summer and fall CESM and NorESM generally produce higher concentrations of BC than CanAM and SMHI-MATCH throughout the entire depth of the troposphere (i.e. 1000-250 hPa), consistent with higher Arctic BC burdens in these models. Similarly, persistent high concentrations in the upper troposphere/stratosphere (i.e. 250-10 hPa) during fall and winter in NorESM, and to lesser extent in CESM, are not reproduced by CanAM (Fig. 4c).

Lower simulated upper tropospheric/stratospheric concentrations in CanAM than in CESM or NorESM are consistent with higher BC burdens and shorter BC wet deposition time scales in CanAM outside the Arctic (see Fig. S1) since clouds with notable precipitation rarely occur in the upper troposphere in the Arctic. Owing to the high static stability of the Arctic atmosphere, high aerosol concentrations in the upper troposphere/lower stratosphere in CESM and NorESM are likely related to advection of BC to the Arctic following isentropic surfaces from lower latitudes. Vertical transport of BC by sporadically occurring deep convection in the Arctic are unlikely to contribute to

concentrations in the upper troposphere/lower stratosphere, as will be discussed in more detail later. Consequently, differences in upper tropospheric BC concentrations and burdens in simulations appear to be related to differences in simulated large-scale lifting of air masses or convective transport of BC outside the Arctic. This is broadly consistent with *Allen and Landuyt* [2014] who found that CMIP5 climate models tend to produce higher concentrations of BC in the upper troposphere and lower stratosphere (UT/LS) than observed from aircraft. A modified version of one of the models in their study with reduced convective transport of BC produced lower concentrations and better agreement with observations in the UT/LS outside the Arctic. However, underestimates in BC concentrations in the Arctic become more pronounced with reduced convective transport.

In order to understand the role of convective processes on BC concentrations and burdens in the Arctic region, we conducted a number of sensitivity experiments (see Table 5). For CONV_WD, in-cloud removal of BC was disabled in the model (convective wet removal solubility factor of 0). This modification leads to more efficient convective transport of BC in convective updrafts in the models compared to the original simulation, hereafter referred to as CNTRL (Fig. 5). We also conducted another sensitivity experiment by completely turning off the convective transport calculations for BC (CONV_TR), which disables transport of BC by convective updrafts, downdrafts, entrainment, detrainment, compensating subsidence, and convective wet deposition in the model.

Results in Fig. 5 show that CONV_WD produces large amounts of BC in the upper troposphere and stratosphere. As expected, the elimination of convective wet deposition increases the convective transport of BC to higher atmospheric levels by a substantial amount, which illustrates the importance of convective wet deposition for BC burdens in the Arctic both in CanAM (Fig. 5a) and CESM (Fig. 5d). With this modification, CanAM and CESM produce a persistent maximum in upper tropospheric BC concentrations throughout the annual cycle, with similarities to results from NorESM in Fig. 4. Without convective wet removal aerosols can be vertically transported by deep convection from sources near the surface to the mid-/upper troposphere, where these particles are much less affected by wet removal by layer (stratiform) clouds. As a result, they can be transported for a long distance to the Arctic where wet deposition will also be inefficient for these aerosols. Based on these results, it seems likely that differences in convective wet deposition in models exist and that they contribute to differences in simulated BC concentration profiles, with implications for wet deposition removal efficiencies. Note that changes in concentrations in the lower troposphere in CONV_WD are relatively small compared to the upper troposphere so that these will not be analyzed here. Local convective transport in the Arctic appears to be less important for upper tropospheric concentrations than convective transport from regions at lower latitudes. To confirm this we performed one additional sensitivity experiment using CanAM in which the convective wet removal was disabled for regions north of 60°N and found that the impacts of local convective transport in the Arctic are negligible (Fig. S5).

Removal of convective transport of BC (i.e. CONV_TR) produces changes in simulated BC concentrations that are relatively small compared to CONV_WD both in CanAM and CESM (Fig. 5), which indicates that the simulated convection mainly acts to clean the atmosphere rather than to redistribute black carbon vertically. In the absence of convective transport and wet removal, the remaining aerosol particles can be transported by large-scale lifting, which makes them susceptible to wet scavenging by stratiform clouds.

Given the substantial magnitude of the simulated impacts, convective wet deposition should be regarded as a key model process for upper tropospheric BC concentrations in the Arctic and elsewhere. Weaker sensitivities in CESM than in CanAM in CONV_WD versus CNTRL indicate that modeling uncertainties exist regarding the efficiency of convective wet deposition, which likely explains at least part of the differences in simulated upper tropospheric BC concentrations among the models in Fig. 5.

In order to determine the extent to which BC concentrations may also be affected by other processes, three additional sensitivity experiments (see Table 5) based on CNTRL were performed. For STF_WD, all wet deposition processes for BC in layer clouds were turned off. For DRYD, dry deposition and gravitational settling were turned off. Finally, aging of externally mixed, hydrophobic BC to internally mixed, hydrophilic BC-containing particles was disabled in AGE.

As expected, BC burdens are increased in CanAM and CESM in STF_WD, with generally weaker increases in CESM than in CanAM (Tables S3 and S4; Fig. S6). An associated increase in BC lifetime is most pronounced during summer and fall, with overall little changes in the upper troposphere. In CanAM, the seasonal cycle in STF_WD has a maximum in summer in the troposphere, with a seasonal cycle that is very different from CNTRL. Changes in seasonality are less pronounced for CESM, which may be related to differences in parameterizations of wet deposition or properties (size and hygroscopicity) of the aerosol in the models. This indicates that the wet removal by stratiform precipitation strongly impacts the seasonal cycle of near-surface BC concentrations, which is consistent with the finding of Wang et al. (2013) in CESM.

It appears that some of the differences between the CNTRL simulations with CESM, NorESM and CanAM, especially higher BC concentrations in CESM in summer, could potentially be explained by more efficient wet deposition in layer clouds in CanAM compared to CESM and NorESM. However, additional simulations, possibly with modified parameterizations of wet deposition, would be required for a more detailed analysis, which is beyond the scope of the study.

In DRYD, the BC concentration is higher than in CNTRL, especially during winter and spring, with nearly linear increases in BC vertical distributions. However, differences between DYRD and CNTRL are relatively small compared to other sensitivity tests. Finally, AGE combines features of STF_WD and CONV_WD since aging of BC from

hydrophobic to hydrophilic is important for in-cloud removal in layer as well as convective clouds. Consequently, BC concentrations are increased throughout the full depth of the atmosphere (Fig 5a) and seasonal variations in concentrations and burdens are opposite to CNTRL in CanAM (Figs. 5b, 5c and 6S), but weaker than in STF_WD. CESM produces a much larger increase in BC burdens in AGE than CanAM (Fig. 6S). In order to understand these differences, consider that wet deposition is less efficient in removing BC from the atmosphere in CESM than in CanAM (Tables S3 and S4; Fig. S7). In CanAM, all of the BC biomass burning emissions and 20% of emissions from fossil fuel burning, aircraft and shipping are assumed to be hygroscopic and therefore subject to wet deposition near emission sources whereas in CESM all of the newly emitted BC is assumed to be hydrophobic and thus not subject to wet deposition if not mixed with hygroscopic species, which causes relatively small impacts of atmospheric aging processes on BC burdens in CanAM compared to CESM.

In summary, CanAM and CESM both produce higher BC burdens in all of the sensitivity experiments compared to the corresponding CNTRL simulations (Fig. S6). However, there are substantial differences in terms of the magnitude and seasonality of the burdens in the experiments (Fig. S6). For CanAM, stratiform wet deposition, aging processes, and convective wet deposition (experiments STF_WD,AGE, CONV_WD, respectively) clearly contribute to the simulated seasonal variations in BC burdens in the CNTRL simulations, with high BC burdens in spring and low BC burdens in fall (Figs. 5 and S6). For CESM, stratiform wet deposition has a much weaker impact on seasonal

variation of BC burdens (Figs. 5 and S6). However, impacts of aging and convective wet deposition on seasonal variations are also large for CESM. Convective wet deposition has a greater impact on BC burdens in CanAM than in CESM whereas aging of BC in the atmosphere produces weaker impacts in CanAM. Furthermore, DRYD and CONV_TR essentially reproduce the seasonality in CNTRL which implies that impacts of dry deposition and convective transport on seasonal variations in BC burdens are small in CanAM and CESM.

Although not directly comparable, results from the sensitivity experiments are broadly consistent with results from calculations with the simple conceptual model in Section 3.3. In particular, both give evidence for large impacts of wet deposition in the Arctic on the amounts and seasonality of BC in the Arctic. The removal of total wet deposition from the conceptual model (Section 3.3) and stratiform wet deposition from full 3D models (this section) leads to much higher BC burdens and relatively weak seasonal reductions, or even increases, in simulated BC burdens between spring and fall. Results from the sensitivity tests with the full 3D models indicate that differences in stratiform wet deposition in CanAM and CESM are mainly associated with precipitating clouds below 250 hPa (Figs. 4 and 5). The removal of stratiform wet deposition from CESM produces a weaker impact on BC burden and seasonality compared to CanAM. Given the good agreement between simulated springtime BC concentrations and precipitation rates in the models it seems possible that differences in simulated wet

deposition time scales may be associated with parameterizations of microphysical aerosol/cloud interactions rather than parameterizations of precipitation processes.

In addition, according to results from the sensitivity tests with full 3D models, differences in the efficiency of stratiform wet deposition in CanAM and CESM are also related to differences in convective wet deposition in these models. The removal of convective wet deposition leads to longer residence times of BC in the Arctic atmosphere, especially for CanAM (Tables S3 and S4). Without efficient convective wet deposition, concentrations of BC tend to be higher in the upper troposphere and stratosphere. However, stratiform wet deposition mainly occurs in the lower troposphere, with low precipitation rates for upper tropospheric clouds (not shown). Unfortunately, sensitivity tests with NorESM are not available so that we can only speculate that the particularly low efficiency of wet deposition in the Arctic in NorESM might be associated with inefficient convective wet deposition compared to the other models. In contrast to impacts of wet deposition on model results, impacts of dry deposition on BC burdens are relatively weak according to simulations with conceptual and full 3D models.

4 Conclusions

Typically, near-surface BC concentrations in the Arctic vary substantially over the course of a year. Seasonal variations in BC concentrations depend on changes in Arctic BC processes and long-range transport of BC to the Arctic. Since BC emissions in the Arctic are low and dry deposition is relatively inefficient, BC burdens in the Arctic are

largely determined by transport and wet deposition. The current study provides a new framework for diagnosing relationships between key processes for Arctic BC burdens. Results from three global climate models and one chemistry transport model were used. These models were recently used to assess impacts of BC on Arctic climate by the expert group on black carbon and ozone, Arctic Monitoring and Assessment Programme [*AMAP*, 2015: *Sand et al*., 2015].

Simulated BC burdens and mass budgets in the models agree well over the main source regions. However, significant differences exist in remote regions, especially the Arctic. All models produce net positive transport to the Arctic throughout the year. The maximum BC transport occurs in July while the minimum transport is in May in the models. In July, forest fires near ~60°N contribute significantly to the overall transport of BC to the Arctic region (>67°N). Similarly on a seasonal basis, the largest transport occurs during summer, followed by winter and spring. However, there is little agreement in the simulated seasonality of BC burdens among the models. CanAM, SMHI-MATCH and CESM show strong seasonal changes in burdens while NorESM has the weakest seasonal cycle among the models. The latter also produces higher burdens than the other models, especially compared to CanAM. NorESM and CESM in general produce large amounts of BC in the upper troposphere with substantially longer residence time of BC compared to other models, especially in the Arctic.

Relative roles of wet and dry deposition rates change over the course of the year. In the model mean, wet and dry deposition rates are similar in winter and wet deposition dominates the loss of BC from the Arctic atmosphere in other seasons, with a maximum efficiency of wet deposition in summer and fall. There are relatively small variations in the magnitude of wet deposition efficiency in SMHI-MATCH during different seasons. However, the dry deposition in this model also becomes relatively more important during the winter season, similar to other models.

Simulations with a simple conceptual model of BC mass budgets, constrained by diagnosed sources and sinks from simulations with the AMAP models, gave evidence for large sensitivity of changes in BC burdens between spring and fall to transport of BC to the Arctic and wet deposition. Differences in dry deposition or emissions in the Arctic were shown to be of minor importance for BC burden changes.

In order to understand which aerosol processes contribute to vertical distributions and seasonal variations of BC in the Arctic, we performed a series of sensitivity experiments with individual processes switched off using CanAM and CESM. The results from these experiments indicate that differences in simulated BC concentrations in the upper troposphere can largely be attributed to differences in the efficiency of BC scavenging in convective clouds outside the Arctic. Versions of the models that did not account for scavenging of aerosols in convective clouds produced much higher concentrations with relatively weak seasonal variations in the upper troposphere and stratosphere, where the

largest model differences occur. In addition, the efficiency of wet deposition in layer (stratiform) clouds partly explains some of the differences in lower tropospheric BC concentrations in the models.

In contrast to *Allen and Landuyt* [2014], who concluded that convective mass fluxes of BC to the upper troposphere may be overestimated in models, we only find a weak dependence of BC concentrations on convective mass fluxes in sensitivity experiments using CanAM and CESM without convective transport of BC. This is because the highly efficient scavenging of BC in convective clouds reduces the efficiency of convective detrainment of BC into the mid and upper troposphere in the present study. We only consider impacts of convective transport on aerosols whereas *Allen and Landuyt* [2014] additionally account for impacts of convective transport on the simulated hydrological cycle, which may explain the weaker sensitivity of model results to convective transport in our study compared to *Allen and Landuyt* [2014].

We also found that wet deposition in stratiform clouds and dry deposition play an important role for simulations of BC concentrations in the lower troposphere and therefore BC burdens. In particular, simulations with CanAM without wet deposition in layer clouds produced a very different seasonal cycle of BC concentrations in the lower troposphere, with substantially higher concentrations in summer than in the control simulation. In comparison, impacts of dry deposition on the seasonal cycle of BC concentrations are much smaller.

Overall, the current study highlights key differences in simulated BC burdens in the Arctic which are directly relevant to studies of Arctic pollution and climate. In particular, parameterizations of convective wet deposition in models were shown to have large impacts on simulated BC burdens. Conceptually very different parameterizations of convective processes are used in the AMAP models considered here and in other models. Future studies should therefore focus on these parameterizations in order to improve models of Arctic BC and climate.

***Acknowledgement*: We thank five anonymous reviewers for helpful comments and support.** This study was partly supported by NSERC through the Canadian NETCARE research network and by the Arctic Monitoring and Assessment Programme (AMAP). M. Flanner acknowledges support from AMAP and the U.S. Department of Energy (DOE) award number DE-SC0013991. H. Wang acknowledges support from the DOE, Office of Science, Biological and Environmental Research as part of the Earth System Modeling Program. The Pacific Northwest National Laboratory (PNNL) is operated for DOE by Battelle Memorial Institute under contract DE-AC05-76RLO1830. Contributions by SMHI were funded by the Swedish Environmental Protection Agency under contract NV-09414-12 and through the Swedish Clean Air & Climate research program, SCAC. We are thankful to other members of the AMAP Expert Group on black carbon and ozone for their support of model simulations and discussions. We also thank Richard Leaitch and Marie-Ève Gagné for comments on the manuscript. Data sets are accessible via anonymous ftp file transfer from ftp.cccma.ec.gc.ca in the directory

/pub/AMAP/model_intercomparison. In addition, scripts that were used to process these data sets are available from the corresponding author upon request (Email: knut.vonsalzen@canada.ca).

References

Allen, R. J., and W. Landuyt (2014), The vertical distribution of black carbon in CMIP5 models: Comparison to observations and the importance of convective transport, *J. Geophys. Res. Atmos.*, **119**, 4808-4835, doi:10.1002/2014JD021595.

AMAP (2015), AMAP Assessment 2015: Black carbon and ozone as Arctic climate forcers. Arctic Monitoring and Assessment Programme (AMAP), Oslo, Norway. vii + 116 pp., http://www.amap.no/documents/doc/AMAP-Assessment-2015-Black-carbon-and-ozone-as-Arctic-climate-forcers/1299

Andersson, C., J. Langner, and R. Bergstrom (2007), Interannual variation and trends in air pollution over Europe due to climate variability during 1958–2001 simulated with a regional CTM coupled to the ERA40 reanalysis, *Tellus Ser.B*, **59**, 77–98, doi: 10.1111/j.1600-0889.2006.00196.x

Barrie, L. A. (1986), Arctic air pollution – An overview of current knowledge, *Atmospheric Environment*, **20**, 643- 663.

Barth, M. C., P. J. Rasch, J. T. Kiehl, C. M. Benkovitz, and S. E. Schwartz (2000), Sulfur chemistry in the National Center for Atmospheric Research Community Climate

Model: Description, evaluation, features and sensitivity to aqueous chemistry, *J. Geophys. Res.*, **105**, 1387–1415. doi:10.1029/1999JD900773.

Bentsen, M., I. Bethke, J. B. Debernard, T. Iversen, A. Kirkevåg, Ø. Seland, H. Drange, C. Roelandt, I. A. Seierstad, C. Hoose, and J. E. Kristjánsson (2013), The Norwegian Earth System Model, NorESM1-M – Part 1: Description and basic evaluation of the physical climate, *Geosci. Model Dev.*, **6**, 687-720, doi:10.5194/gmd-6-687-2013.

Bond, T. C., and R. W. Bergstrom (2006), Light absorption by carbonaceous particles: An investigative review, *Aerosol Science and Technology*, **40**, 27-67, doi:10.1080/02786820500421521.

Bond, T. C., D. G. Streets, K. F. Yarber, S. M. Nelson, J. H. Woo, and Z. Klimont (2004), A technology-based global inventory of black and organic carbon emissions from combustion, *J. Geophys. Res.*, **109,** D14203, doi:10.1029/2003JD003697.

Bond, T. C., et al. (2013), Bounding the role of black carbon in the climate system: A scientific assessment, *J. Geophys. Res. Atmos.*, **118**, 5380-5552, doi:10.1002/jgrd.50171.

Boucher, O., D. Randall, P. Artaxo, C. Bretherton, G. Feingold, P. Forster, V. -M. Kerminen, Y. Kondo, H. Liao, U. Lohmann, P. Rasch, S. K. Satheesh, S. Sherwood, B. Stevens and X. Y. Zhang (2013), Clouds and Aerosols. In: Climate Change 2013: The Physical Science Basis. Contribution of Working Group I to the Fifth Assessment Report of the Intergovernmental Panel on Climate Change [Stocker,

T.F., D. Qin, G. -K. Plattner, M. Tignor, S. K. Allen, J. Boschung, A. Nauels, Y. Xia, V. Bex and P. M. Midgley (eds.)], Cambridge University Press, Cambridge, United Kingdom and New York, NY, USA.

Browse, J., K. S. Carslaw, S. R. Arnold, K. Pringle, and O. Boucher (2012), The scavenging processes controlling the seasonal cycle in Arctic sulphate and black carbon aerosol, *Atmos. Chem. Phys.*, **12**, 6775-6798, doi:10.5194/acp-12-6775-2012.

Cachier, H., M. Bremond, and P. Buat-Menard (1989), Determination of atmospheric soot carbon with a simple thermal method, *Tellus*, *Ser. B*, **41**, 379 – 390.

Eckhardt, S., B. Quennehen, D. J. L. Olivié, T. K. Berntsen, R. Cherian, J. H. Christensen, W. Collins, S. Crepinsek, N. Daskalakis, M. Flanner, A. Herber, C. Heyes, Ø. Hodnebrog, L. Huang, M. Kanakidou, Z. Klimont, J. Langner, K. S. Law, M. T. Lund, R. Mahmood, A. Massling, S. Myriokefalitakis, I. E. Nielsen, J. K. Nøjgaard, J. Quaas, P. K. Quinn, J. -C. Raut, S. T. Rumbold, M. Schulz, S. Sharma, R. B. Skeie, H. Skov, T. Uttal, K. von Salzen, and A. Stohl (2015), Current model capabilities for simulating black carbon and sulfate concentrations in the Arctic atmosphere: a multi-model evaluation using a comprehensive measurement data set, *Atmos. Chem. Phys.*, **15**, 9413-9433, doi:10.5194/acp-15-9413-2015.

Garrett, T. J., C. Zhao, and P. C. Novelli (2010), Assessing the relative contributions of transport efficiency and scavenging to seasonal variability in Arctic aerosol, *Tellus*, *Ser. B*, **62**, 190–196, doi:10.1111/j.1600-0889.2010.00453.x.

Garrett, T. J., S. Brattström, S. Sharma, D. E. J. Worthy, and P. Novelli (2011), The role of scavenging in the seasonal transport of black carbon and sulfate to the Arctic, *Geophys. Res. Lett*., **38**, L16805, doi:10.1029/2011GL048221.

Genberg, J., H. A. C. Denier van der Gon, D. Simpson, E. Swietlicki, H. Areskoug, D. Beddows, D. Ceburnis, M. Fiebig, H. C. Hansson, R. M. Harrison, S. G. Jennings, S. Saarikoski, G. Spindler, A. J. H. Visschedijk, A. Wiedensohler, K. E. Yttri, and R. Bergström (2013), Light-absorbing carbon in Europe – measurement and modelling, with a focus on residential wood combustion emissions, *Atmos. Chem. Phys*., **13**, 8719-8738, doi:10.5194/acp-13-8719-2013.

Hansen, A. D. A., H. Rosen, and T. Novakov (1984), The aethalometer—An instrument for the real-time measurement of optical absorption by aerosol particles, *Sci. Total Environ*., **36**, 191– 196.

Hansen, J., and L. Nazarenko (2004), Soot climate forcing via snow and ice albedos, *P. Natl. Acad. Sci. USA*, **101**(2), 423-428, doi:10.1073/pnas.2237157100.

Hansen, J., M. Sato, and R. Ruedy (1997), Radiative forcing and climate response, *J. Geophys. Res*., **102**, 6831-6864.

Hodnebrog, Ø., G. Myhre, and B. H. Samset, (2014), How shorter black carbon lifetime alters its climate effect, *Nat. Commun*., **5**, 5065, doi: 1D.1038/ncomms6065.

Iversen, T., and Ø. Seland (2002), A scheme for process-tagged SO4 and BC aerosols in NCAR-CCM3, Validation and sensitivity to cloud processes, *J. Geophys. Res*., **107**, 4751, doi:10.1029/2001JD000885.

Iversen, T., and Ø. Seland (2003), Correction to "A scheme for process-tagged SO4 and BC aerosols in NCAR-CCM3, Validation and sensitivity to cloud processes", *J. Geophys. Res*., **108**, 4502, doi:10.1029/2003JD003840.

Jocobson, M. Z. (2001), Strong radiative heating due to the mixing state of black carbon in the atmospheric aerosols, *Nature*, **409**, 695-698.

Kipling, Z., P. Stier, C. E. Johnson, G. W. Mann, N. Bellouin, S. E. Bauer, T. Bergman, M. Chin, T. Diehl, S. J. Ghan, T. Iversen, A. Kirkevåg, H. Kokkola, X. Liu, G. Luo, T. van Noije, K. J. Pringle, K. von Salzen, M. Schulz, Ø. Seland, R. B. Skeie, T. Takemura, K. Tsigaridis, and K. Zhang (2015), What controls the vertical distribution of aerosol? Relationships between process sensitivity in HadGEM3–UKCA and inter-model variation from AeroCom Phase II, *Atmos. Chem. Phys. Discuss*., **15**, 25933-25980, doi:10.5194/acpd-15-25933-2015.

Kipling, Z., P. Stier, J. P. Schwarz, A. E. Perring, J. R. Spackman, G. W. Mann, C. E. Johnson, and P. J. Telford (2013), Constraints on aerosol processes in climate models from vertically-resolved aircraft observations of black carbon, *Atmos. Chem. Phys*., **13**, 5969-5986, doi:10.5194/acp-13-5969-2013.

Kirkevåg, A., et al. (2013), Aerosol–climate interactions in the Norwegian Earth System Model – NorESM1-M, *Geosci. Model Dev*., **6**(1), 207–244, doi:10.5194/gmd-6-207-2013.

Koch, D., M. Schulz, S. Kinne, C. McNaughton, J. R. Spackman, Y. Balkanski, S. Bauer, T. Berntsen, T. C. Bond, O. Boucher, M. Chin, A. Clarke, N. De Luca, F. Dentener,

T. Diehl, O. Dubovik, R. Easter, D. W. Fahey, J. Feichter, D. Fillmore, S. Freitag, S. Ghan, P. Ginoux, S. Gong, L. Horowitz, T. Iversen, A. Kirkevag, Z. Klimont, Y. Kondo, M. Krol, X. Liu, R. Miller, V. Montanaro, N. Moteki, G. Myhre, , J. E. Penner, J. Perlwitz, G. Pitari, S. Reddy, L. Sahu, , H. Sakamoto, G. Schuster, J. P. Schwarz, O. Seland, , P. Stier, N. Takegawa, T. Takemura, C. Textor, J. A. van Aardenne, and Y. Zhao (2009), Evaluation of black carbon estimations in global aerosol models, *Atmos. Chem. Phys.*, **9**, 9001-9026.

Koch, D., Y. Balkanski, S. E. Bauer, R. C. Easter, S. Ferrachat, S. J. Ghan, C. Hoose, T. Iversen, A. Kirkevåg, J. E. Kristjansson, X. Liu, U. Lohmann, S. Menon, J. Quaas, M. Schulz, Ø. Seland, T. Takemura, and N. Yan (2011), Soot microphysical effects on liquid clouds, a multi-model investigation, *Atmos. Chem. Phys.*, **11**, 1051-1064, doi:10.5194/acp-11-1051-2011.

Liu, J., S. Fan, L. W. Horowitz, and H. Levy II (2011), Evaluation of factors controlling long-range transport of black carbon to the Arctic, *J. Geophys. Res.*, **116**, D04307, doi:10.1029/2010JD015145.

Liu, X., P.-L. Ma, H. Wang, S. Tilmes, B. Singh, R. C. Easter, S. J. Ghan, and P. J. Rasch (2016), Description and evaluation of a new 4-mode version of Modal Aerosol Module (MAM4) within version 5.3 of the Community Atmosphere Model, Geoscientific Model Development, **9**, 505-522, doi:10.5194/gmd-9-505-2016.

Liu, X., R. C. Easter, S. J. Ghan, R. Zaveri, P. Rasch, X. Shi, J.-F. Lamarque, A. Gettelman, H. Morrison, F. Vitt, A. Conley, S. Park, R. Neale, C. Hannay, A. M. L.

Ekman, P. Hess, N. Mahowald, W. Collins, M. J. Iacono, C. S. Bretherton, M. G. Flanner, and D. Mitchell (2012), Toward a minimal representation of aerosols in climate models: description and evaluation in the Community Atmosphere Model CAM5, *Geosci. Model Dev.*, **5**, 709-739, doi:10.5194/gmd-5-709-2012.

Ma, P.-L., P. J. Rasch, H. Wang, K. Zhang, R. C. Easter, S. Tilmes, J. D. Fast, X. Liu, J.-H. Yoon, and J.-F. Lamarque (2013), The role of circulation features on black carbon transport into the Arctic in the Community Atmosphere Model version 5 (CAM5), *J. Geophys. Res.*, **118**, 4657–4669, doi:10.1002/jgrd.50411.

Ma, P.-L., P. J. Rasch, J. D. Fast, R. C. Easter, W. I. Gustafson Jr., X. Liu, S. J. Ghan, and B. Singh (2014), Assessing the CAM5 physics suite in the WRF-Chem model: Implementation, resolution sensitivity, and a first evaluation for a regional case study, Geoscientific Model Development, **7**, 755-778, doi:10.5194/gmd-7-755-2014.

Neale, R. B., C. -C. Chen, A. Gettelman, P. H. Lauritzen, S. Park, D. L. Williamson, A. J. Conley, R. Garcia, D. Kinnison, J. -F. Lamarque, D. Marsh, M. Mills, A. K. Smith, S. Tilmes, F. Vitt, H. Morrison, P. Cameron-Smith, W. D. Collins, M. J. Iacono, R. C. Easter, S. J. Ghan, X. Liu, P. J. Rasch, and M. A. Taylor (2012), Description of the NCAR Community Atmosphere Model (CAM5.0), NCAR Technical Note, http://www.cesm.ucar.edu/models/cesm1.0/cam/docs/description/cam5_desc.pdf.

Ramshaw, J. D. (1985), Conservative rezoning algorithm for generalized two-dimensional meshes. *J. Comp. Phys.*, 59, 193-199. doi:10.1016/0021-9991(85)90141-X .

Rasch, P. J., M. C. Barth, J. T. Kiehl, S. E. Schwartz, and C. M. Benkovitz (2000), A description of the global sulfur cycle and its controlling processes in the National Center for Atmospheric Research Community Climate Model, Version 3, *J. Geophys. Res*., **105**, 1367–1385.

Real, E., E. Orlandi, K. S. Law, F. Fierli, D. Josset, F. Cairo, H. Schlager, S. Borrmann, D. Kunkel, C. M. Volk, J. B. McQuaid, D. J. Stewart, J. Lee, A. C. Lewis, J. R. Hopkins, F. Ravegnani, A. Ulanovski, and C. Liousse (2010), Cross-hemispheric transport of central African biomass burning pollutants: implications for downwind ozone production, *Atmos. Chem. Phys*., **10**, 3027-3046.

Robertson, L., J. Langner, and M. Engardt (1999), An Eulerian limited-area atmospheric transport model, *J. Appl. Met*., **38**, 190–210.

Samset, B. H., G. Myhre, A. Herber, Y. Kondo, S. -M. Li, N. Moteki, M. Koike, N. Oshima, J. P. Schwarz, Y. Balkanski, S. E. Bauer, N. Bellouin, T. K. Berntsen, H. Bian, M. Chin, T. Diehl, R. C. Easter, S. J. Ghan, T. Iversen, A. Kirkevåg, J. -F. Lamarque, , G. Lin, X. Liu, J. E. Penner, M. Schulz, Ø. Seland, R. B. Skeie, P. Stier, T. Takemura, K. Tsigaridis, and K. Zhang (2014), Modelled black carbon radiative forcing and atmospheric lifetime in AeroCom Phase II constrained by aircraft

observations, *Atmos. Chem. Phys*., **14**, 12465-12477, doi:10.5194/acp-14-12465-2014.

Sand, M., T. Berntsen, K. von Salzen, M. Flanner, J. Langner, and D. Victor (2015), Response of Arctic temperature to changes in emissions of short-lived climate forcers, *Nature Climate Change*, doi: 10.1038/NCLIMATE2880.

Sand, M., T. K. Berntsen, Ø. Seland, and J. E. Kristja´nsson (2013), Arctic surface temperature change to emissions of black carbon within Arctic or midlatitudes, *J. Geophys. Res. Atmos*., **118**, 7788–7798, doi:10.1002/jgrd.50613.

Sawa, Y., T. Machida, and H. Matsueda (2012), Aircraft observation of the seasonal variation in the transport of CO2 inthe upper atmosphere, *J. Geophys. Res*., **117**, D05305, doi:10.1029/2011JD016933.

Seland, Ø., T. Iversen, A. Kirkev ag, and T. Storelvmo (2008), Aerosol-climate interactions in the CAM-Oslo atmospheric GCM and investigations of associated shortcomings, *Tellus Ser.A*, **60**, 459–49.

Sharma, S., E. Andrews, L. A. Barrie, J. A. Ogren, and D. Lavoué (2006), Variations and sources of the equivalent black carbon in the high Arctic revealed by long-term observations at Alert and Barrow: 1989-2003, *J. Geophys. Res*., **111,** D14208, doi: 10.1029/2005JD006581.

Sharma, S., M. Ishizawa, D. Chan, D. Lavoue´, E. Andrews, K. Eleftheriadis, and S. Maksyutov (2013), 16-year simulation of Arctic black carbon: Transport, source

contribution, and sensitivity analysis on deposition, *J. Geophys. Res. Atmos*., **118**, 943–964, doi:10.1029/2012JD017774.

Shindell, D. T., M. Chin, F. Dentener, R. M. Doherty, G. Faluvegi, A. M. Fiore, P. Hess, D. M. Koch, I. A. MacKenzie, M. G. Sanderson, M. G. Schultz, M. Schulz, D. S. Stevenson, H. Teich, C. Textor, O. Wild, D. J. Bergmann, I. Bey, H. Bian, C. Cuvelier, B. N. Duncan, G. Folberth, L. W. Horowitz, J. Jonson, J. W. Kaminski, E. Marmer, R. Park, K. J. Pringle, S. Schroeder, S. Szopa, T. Takemura, G. Zeng, T. J. Keating, and A. Zuber (2008), A multi-model assessment of pollution transport to the Arctic, *Atmos. Chem. Phys*., **8**, 5353-5372, doi:10.5194/acp-8-5353-2008.

Staudt, A.C., D. J. Jacob, J. A. Logan, D. Bachiochi, T. N. Krishnamurti, and G. W. Sachse (2001), Continental sources, transoceanic transport, and interhemispheric exchange of carbon monoxide over the Pacific, *J. Geophys. Res*., **106**, 32571-32589.

Stohl, A. (2006), Characteristics of atmospheric transport into the Arctic troposphere, *J. Geophys. Res*., **111,** D11306, doi:10.1029/2005JD006888.

Stohl, A., B. Aamaas, M. Amann, L. H. Baker, N. Bellouin, T. K. Berntsen, O. Boucher, R. Cherian, W. Collins, N. Daskalakis, M. Dusinska, S. Eckhardt, J. S. Fuglestvedt, M. Harju, C. Heyes, Ø. Hodnebrog, J. Hao, U. Im, M. Kanakidou, Z. Klimont, K. Kupiainen, K. S. Law, M. T. Lund, R. Maas, C. R. MacIntosh, G. Myhre, S. Myriokefalitakis, D. Olivié, J. Quaas, B. Quennehen, J.-C. Raut, S. T. Rumbold, B. H. Samset, M. Schulz, Ø. Seland, K. P. Shine, K. P., R. B. Skeie, S. Wang, K. E.

Yttri, T. Zhu (2015), Evaluating the climate and air quality impacts of short-lived pollutants, *Atmos. Chem. Phys.*, **15**, 10529-10566, doi:10.5194/acp-15-10529-2015.

Sudo, K., and H. Akimoto (2007), Global source attribution of tropospheric ozone: Long-range transport from various source regions, *J. Geophys. Res.*, **112**, D12302, doi:10.1029/2006JD007992.

van der Werf, G. R., J. T. Randerson, L. Giglio, G. J. Collatz, M. Mu, P. S. Kasibhatla, D. C. Morton, R. S. DeFries, Y. Jin, and T. T. van Leeuwen (2010), Global fire emissions and the contribution of deforestation, savanna, forest, agricultural, and peat fires (1997–2009), *Atmos. Chem. Phys.*, **10**, 11707–11735, doi:10.5194/acp-10-11707-2010.

Vignati, E., M. Karl, M. Krol, J. Wilson, P. Stier, and F. Cavalli (2010), Sources of uncertainities in modeling black carbon at global scale, *Atmos. Chem. Phys.*, **10**, 2595–2611.

von Salzen, K. (2006), Piecewise log-normal approximation of size distributions for aerosol modelling, *Atmos. Chem. Phys.*, **6**, 1351-1372.

von Salzen, K., H. G. Leighton, P. A. Ariya, L. A. Barrie, S. L. Gong, J.-P. Blanchet, L. Spacek, U. Lohmann, L. I. Kleinman (2000), Sensitivity of sulphate aerosol size distributions and CCN concentrations over North America to SO_x emissions and H_2O_2 concentrations, *J. Geophys. Res.*, **105**, 9741-9765.

von Salzen, K., J. F. Scinocca, N. A. McFarlane, J. Li, J. N. S. Cole, D. Plummer, D. Verseghy, M. C. Reader, X. Ma, M. Lazare, and L. Solheim (2013), The Canadian

Fourth Generation Atmospheric Global Climate Model (CanAM4). Part I: Representation of Physical Processes, *Atmosphere-Ocean*, **51**, 104-125, doi:10.1080/07055900.2012.755610.

Wang, H., P. J. Rasch, R. C. Easter, B. Singh, R. Zhang, P. -L. Ma, Y. Qian, S. J. Ghan, and N. Beagley (2014), Using an explicit emission tagging method in global modeling of source-receptor relationships for black carbon in the Arctic: Variations, sources, and transport pathways, *J. Geophys. Res. Atmos.*, **119**, 12888–12909, doi:10.1002/2014JD022297.

Wang, H., R. C. Easter, P. J. Rasch, M. Wang, X. Liu, S. J. Ghan, Y. Qian, J. -H. Yoon, P. -L. Ma, and V. Vinoj (2013), Sensitivity of remote aerosol distributions to representation of cloud-aerosol interactions in a global climate model, *Geosci. Model Dev.*, **6**, 765-782, doi:10.5194/gmd-6-765-2013.

Table 1. Model characteristics.

Model (type)	Meteorol. fields	Resolution	Reference
CanAM (GCM), PLA aerosol model	Internal	T63, 49 vertical levels	von Salzen et al. [2013] von Salzen [2006]
CESM (GCM), MAM7 aerosols	Internal	1.9°×2.5°, 30 vertical levels	Liu et al. [2012]
NorESM (GCM), CAM4-Oslo aerosols	Internal	1.9°×2.5°, 26 vertical levels	Bentsen et al. [2013] Kirkevåg et al. [2013]
SMHI-MATCH (CTM)	ECMWF	0.75°×0.75°, 38 vertical levels	Andersson et al. [2007]

Table 2. BC burden (kilotonnes) and radiative forcing (mW/m^2) averaged over the region 60°N to 90°N.

	Burden	Radiative Forcing
CanAM	5.383	307
CESM	7.365	783
NorESM	9.126	808
SMHI-MATCH	5.855	231

(Source: AMAP, 2015)

Table 3. Mean sources and sinks of BC in the Arctic and inferred deposition time scales during time period of simulated declining BC burdens from April 1 to September 30, 2007-2010. Minima and maxima (among the models) are highlighted (bold font). Multi-model mean values (MMM) and model spread (difference between maximum and minimum, in brackets) are provided in the last column.

	CanAM	CESM	NorESM	SMHI-MATCH	MMM (max-min)
Sources and Sinks (kilotonnes)					
Emissions	19.1	15.4	**19.6**	**8.8**	15.7 (10.8)

Transport	27.6	24.2	**30.4**	**24.1**	26.6 (6.3)
Dry deposition	-7.3	-8.7	**-10.3**	**-2.3**	-7.2 (8.0)
Wet deposition	**-43.7**	-33.9	-40.2	**-33.9**	-37.9 (9.8)
Time scales (days)					
Dry deposition	**33.8**	49.5	105.7	**114.9**	76.0 (81.1)
Wet deposition	**5.7**	12.7	**27.2**	7.9	13.4 (21.5)

Table 4. Change in BC burden in the Arctic from April 1 to September 30, 2007-2010 (units: kilotonnes) in the models and sensitivity to variations in strengths of sources and sinks within simulated ranges according to Table 3. Minima and maxima (among the models) are highlighted (bold font). For the minimum and maximum sections of each source or sink term, the burden changes are determined by using minima or maxima of that source or sink term (among the models) highlighted in Table 3. Multi-model mean values (MMM) and model spread (difference between maximum and minimum, in brackets) are provided in the last column.

	CanAM	CESM	NorESM	SMHI-MATCH	MMM (max-min)
Full model	**-4.3**	-3.0	**-0.5**	-3.4	-2.8 (3.8)
Emissions					
removed	**-4.8**	-3.9	**-2.9**	-3.7	-3.8 (1.9)
minimum	**-4.6**	-3.4	**-1.8**	-3.4	-3.3 (2.8)
maximum	**-4.3**	-2.8	**-0.5**	-2.9	-2.6 (3.8)
max-min	0.3	0.6	1.3	0.4	
Transport					
removed	**-5.1**	-4.4	**-4.1**	-4.3	-4.5 (1.0)
minimum	**-4.4**	-3.0	**-1.3**	-3.4	-3.0 (3.1)
maximum	**-4.2**	-2.7	**-0.5**	-3.1	-2.6 (3.7)
max-min	0.2	0.4	0.7	0.3	

Dry deposition						
	removed	**-4.1**	-2.4	**1.0**	-3.3	-2.2 (5.1)
	minimum	**-4.2**	-2.7	**-0.4**	-3.4	-2.7 (3.8)
	maximum	**-4.3**	-3.2	**-2.3**	-3.5	-3.3 (2.0)
	max-min	-0.1	-0.5	-1.9	-0.2	
Wet deposition						
	removed	**3.1**	5.4	**18.5**	12.7	9.9 (15.4)
	minimum	**-1.7**	-1.4	**-0.5**	-0.7	-1.1 (1.2)
	maximum	-4.3	-4.1	**-5.0**	**-3.7**	-4.3 (1.3)
	max-min	-2.6	-2.7	-4.4	-3.0	

Table 5. Summary of sensitivity experiments performed with CanAM and CESM.

Experiment	Modification
CONV_WD	In-cloud removal of BC in deep convection disabled
CONV_TR	Transport of BC in convection disabled
STF_WD	Wet deposition processes for BC in layer clouds disabled
DRYD	Dry deposition and gravitational settling disabled
AGE	Aging of externally mixed, hydrophobic to internally mixed, hydrophilic BC disabled

Figure Captions:

Fig. 1. Seasonal mean BC burden (kilotonnes [kt]) in the Arctic region.

Fig. 2. BC mass budgets for different latitude bands in the models. Note the different y-axis scaling for the Arctic region (top row) and the Antarctic region (5^{th} row). The left y-axis represents net transport and net surface source (kt/day) and the right y-axis represents burden (kt)

Fig. 3. Seasonal mean BC budgets in the Arctic region. Black filled circles represent net source (tranport+emissions minus deposition). The net source values are multiplied by 5 for clarity.

Fig. 4. (a) Annual mean vertical profiles of BC mass mixing ratios (ppb) at Alert, Canada. (b) and (c) Monthly mean vertically integrated BC mass (mg/m^2) for troposphere (1000-250 hPa) and upper troposphere/stratosphere (250-10 hPa) respectively. Note the

different y-axis scales for (b) and (c). For (c) the results from SMHI-MATCH are not included because the necessary data were not available.

Fig. 5. Same as 4 but for the difference between control and sensitivity experiments (experiment –control) in CanAM (a-c) and CESM (d-f). Note the different y-axis scaling for bottom panels.

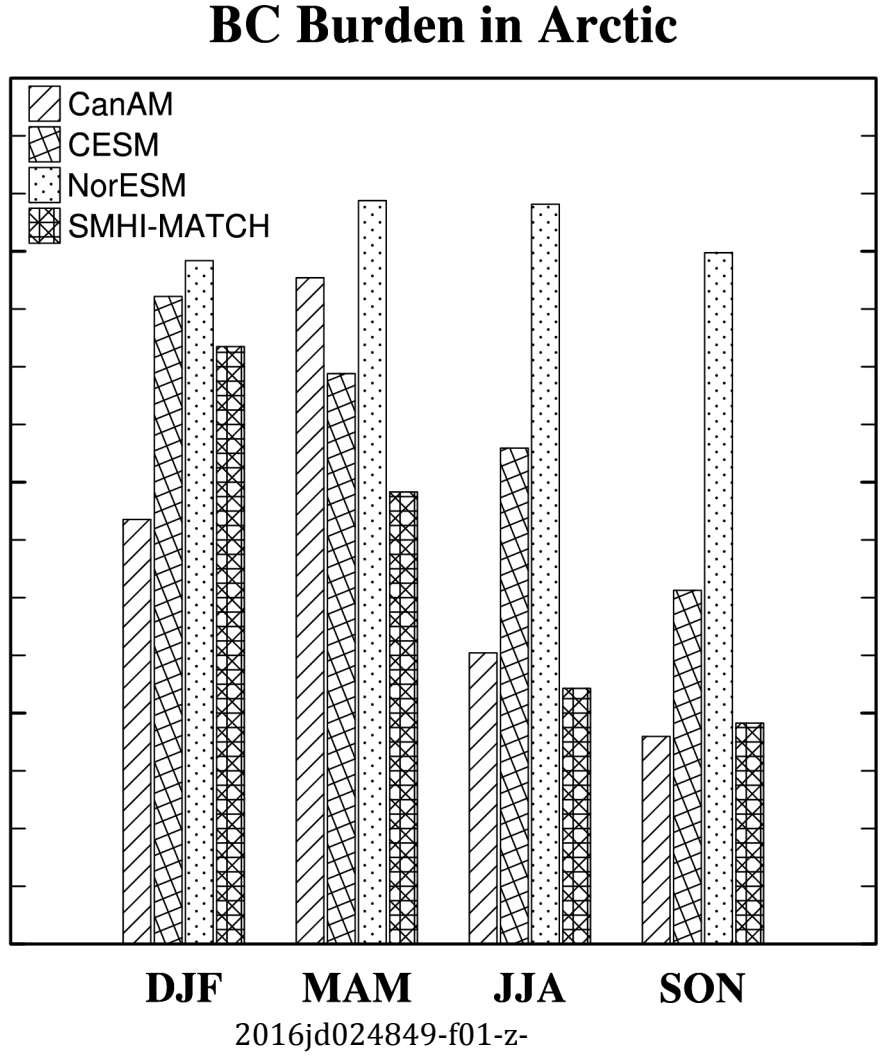

2016jd024849-f01-z-

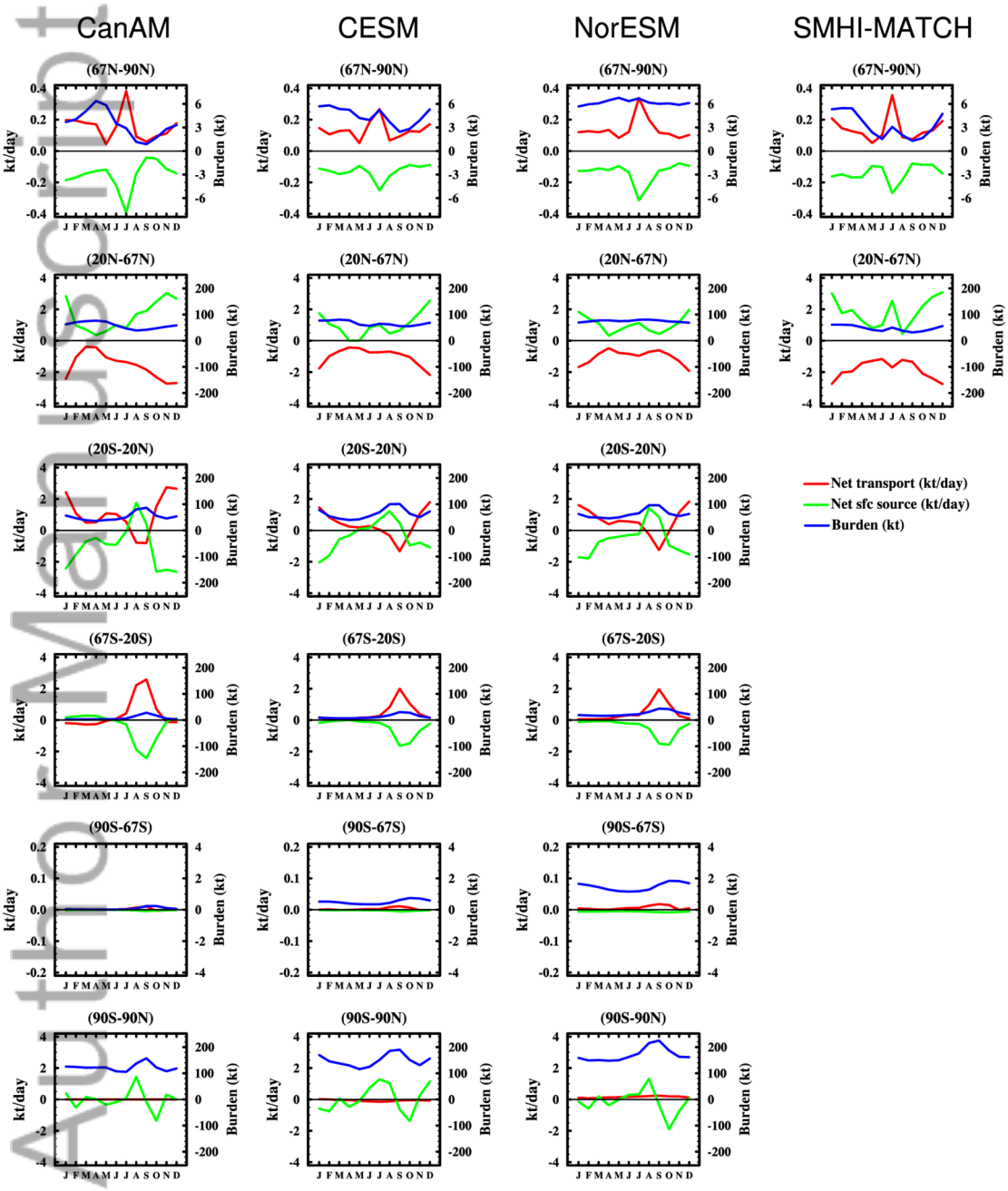

2016jd024849-f02-z-

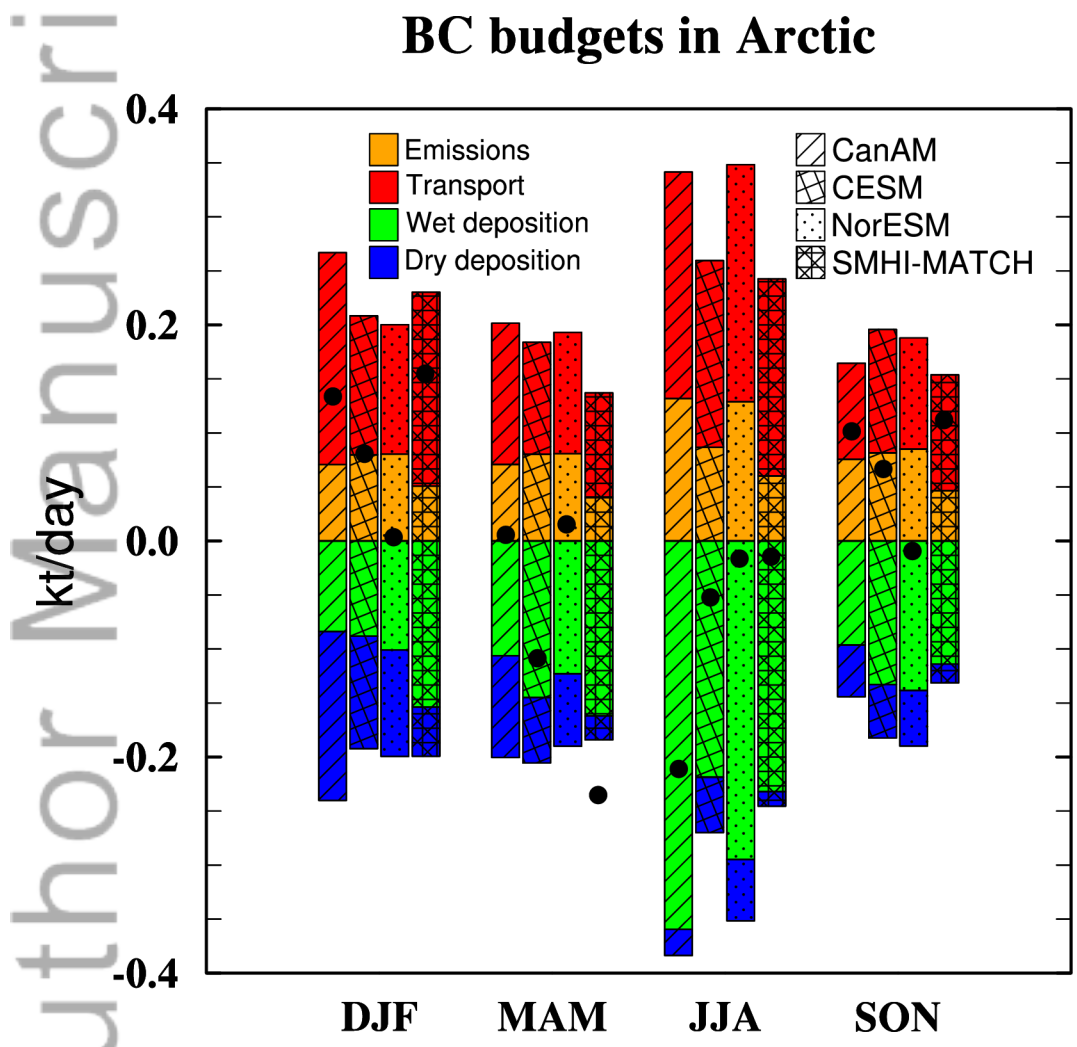

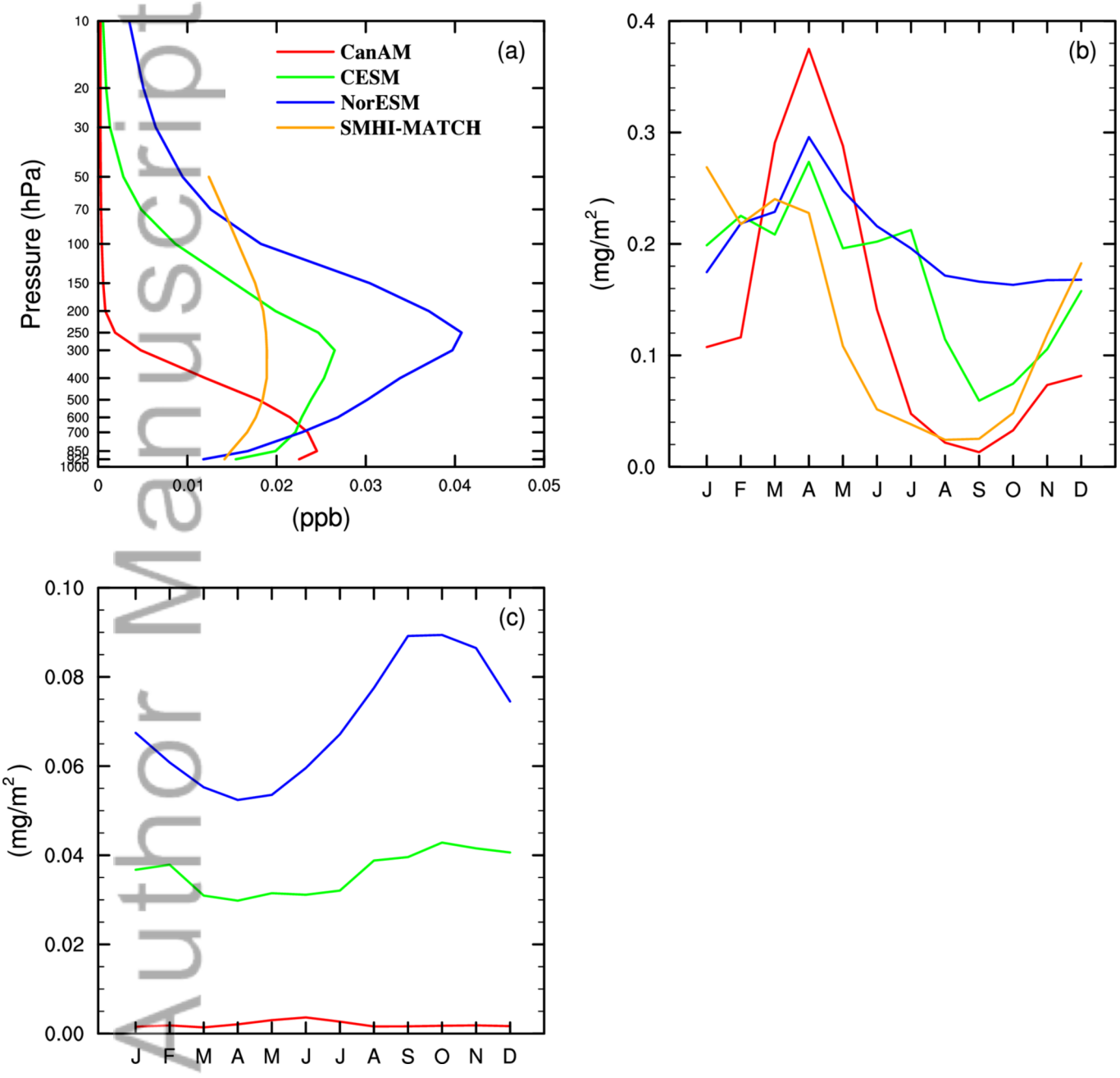

2016jd024849-f04-z-

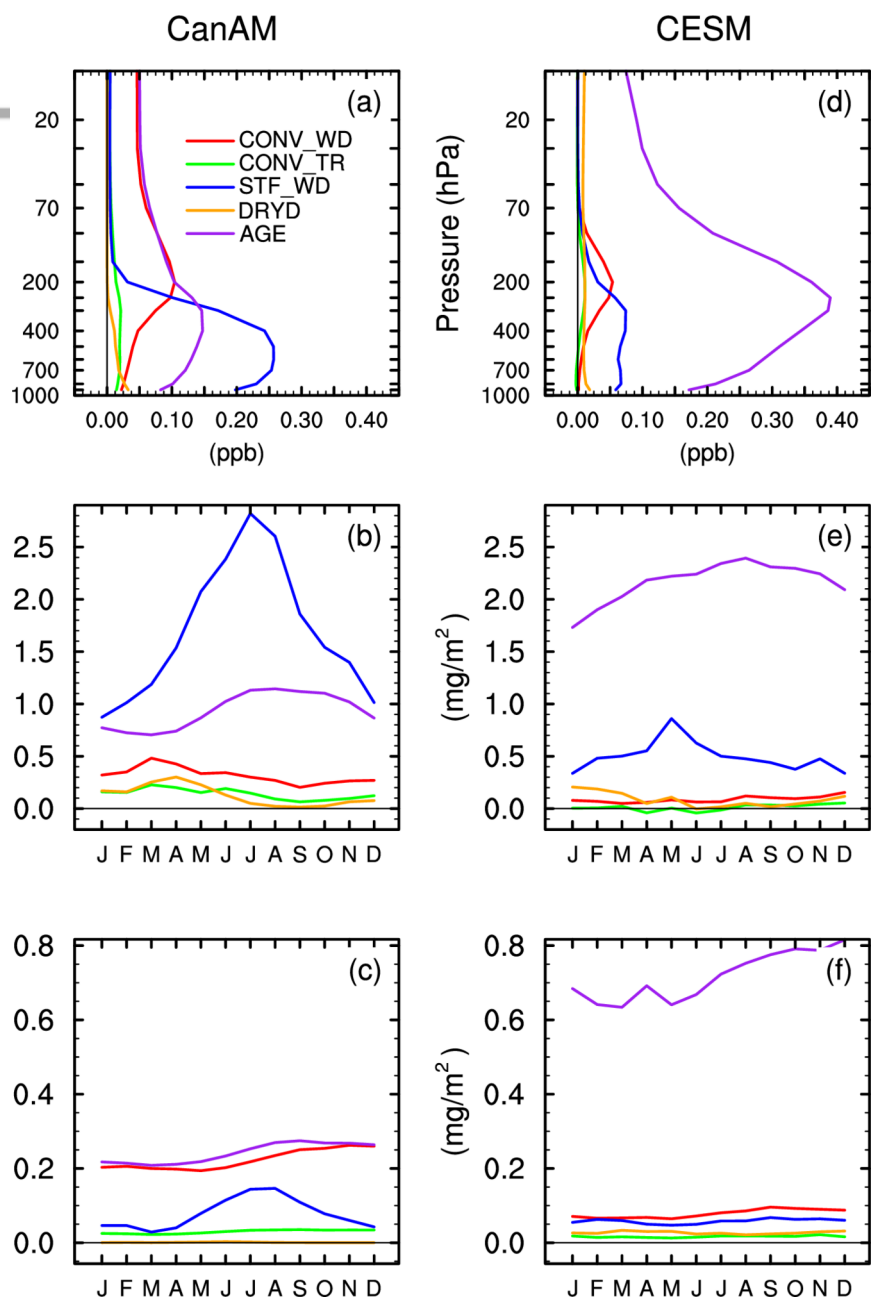

2016jd024849-f05-z-